Received: 3 December 2020 | Revised: 17 February 2021 | Accepted: 12 March 2021

DOI: 10.1002/jbio.202000478

FULL ARTICLE

JOURNAL OF BIOPHOTONICS

Photoacoustic imaging of in vivo hemodynamic responses to sodium nitroprusside

Dong Zhang[1,2] | Ran Li[3,4] | Maomao Chen[2] | Tri Vu[2] | Huaxin Sheng[4] | Wei Yang[4] | Ulrike Hoffmann[4*] | Jianwen Luo[1*] | Junjie Yao[2*]

[1]Department of Biomedical Engineering, School of Medicine, Tsinghua University, Beijing, China

[2]Department of Biomedical Engineering, Duke University, Durham, North Carolina

[3]School of Basic Medical Sciences, North China University of Science and Technology, Tangshan, Hebei, China

[4]Department of Anesthesiology, Duke University School of Medicine, Durham, North Carolina

***Correspondence**
Junjie Yao, Department of Biomedical Engineering, Duke University, Science Dr., Durham, 27710 NC, USA.
Email: junjie.yao@duke.edu

Ulrike Hoffmann, Department of Anesthesiology, Duke University School of Medicine, Research Dr., Durham, 27710 NC, USA.
Email: ulrike.hoffmann@duke.edu

Jianwen Luo, Department of Biomedical Engineering, School of Medicine, Tsinghua University, Shuangqing Rd., 100084 Beijing, China.
Email: luo_jianwen@tsinghua.edu.cn

Funding information
American Heart Association, Grant/Award Number: 18CSA34080277

Abstract

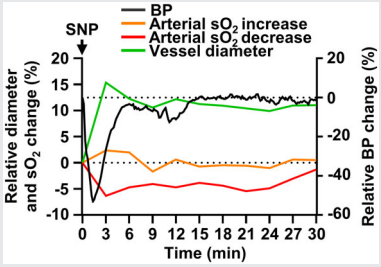

The in vivo hemodynamic impact of sodium nitroprusside (SNP), a widely used antihypertensive agent, has not been well studied. Here, we applied functional optical-resolution photoacoustic microscopy (OR-PAM) to study the hemodynamic responses to SNP in mice in vivo. As expected, after the application of SNP, the systemic blood pressure (BP) was reduced by 53%. The OR-PAM results show that SNP induced an arterial vasodilation of 24% and 23% in the brain and skin, respectively. A weaker venous vasodilation of 9% and 5% was also observed in the brain and skin, respectively. The results show two different types of blood oxygenation response. In mice with decreased blood oxygenation, the arterial and venous oxygenation was respectively reduced by 6% and 13% in the brain, as well as by 7% and 18% in the skin. In mice with increased blood oxygenation, arterial and venous oxygenation was raised by 4% and 22% in the brain, as well as by 1% and 9% in the skin. We observed venous change clearly lagged the arterial change in the skin, but not in the brain. Our results collectively show a correlation among SNP induced changes in systemic BP, vessel size and blood oxygenation.

KEYWORDS

hemodynamics, photoacoustic microscopy, quantitative analysis, sodium nitroprusside

Abbreviations: AL, acoustic lens; AMP, amplifier; BE, beam expander; BOLD, blood-oxygen-level-dependent signals; BP, blood pressure; CBF, cerebral blood flow; ConL, convex lens; CorL, correction lens; DM, dichroic mirror; HbO_2, oxy-hemoglobin; HbR, deoxy-hemoglobin; MRI, magnetic resonance imaging; NA, numerical aperture; NIRS, near-infrared spectroscopy; OR-PAM, optical-resolution photoacoustic microscopy; PAI, photoacoustic Imaging; PET, positron emission tomography; ROI, region of interest; SNP, sodium nitroprusside; sO_2, oxygen saturation of hemoglobin; UT, ultrasound transducer; WT, water tank.

1 | INTRODUCTION

Photoacoustic imaging (PAI), a hybrid technique that ultrasonically detects light absorption, has emerged as a promising modality for preclinical and clinical studies in the last decade [1–7]. PAI, which detects ultrasound waves generated by thermoelastic expansion from light-absorbing tissues, can achieve high contrast, high spatial

resolution, and high sensitivity. Compared with pure optical imaging, PAI can provide higher spatial resolutions in deep tissues, as ultrasound waves are less scattered than light traveling in tissues. PAI has been used to study the structural, functional and molecular information at scales ranging from cells to tissues [8–12]. As a main embodiment of PAI, optical-resolution photoacoustic microscopy (OR-PAM) uses a confocal and coaxial configuration of light excitation and ultrasound detection, with the lateral resolution determined by the tight optical focusing. A two-dimensional (2-D) raster scan enables the volumetric imaging by collecting time-resolved PA signals (A-line) at each location. OR-PAM has been widely used to study the hemodynamic response to various physiological and pathological challenges in small animal models [4, 13–15].

Sodium nitroprusside (SNP), one of the safest and most effective antihypertensive agents [16], causes blood pressure (BP) decrease through nitric oxide mediated vascular smooth muscle relaxation, which leads to vasodilation [17, 18]. SNP has long been used for mitigating hypertension-induced symptoms, such as aortic valve stenosis [19], myocardial infarction [20], pulmonary hypertension [21] and bleeding in surgeries [22]. However, the impact of SNP on the brain vasculature has not been investigated on single vessel levels, especially SNP induced changes in the blood oxygenation levels.

OR-PAM has been used for quantifying blood oxygen saturation (sO_2), an important index for hemodynamic studies [4, 14, 15, 23–25]. Other existing techniques that show potential for noninvasive sO_2 imaging include near-infrared spectroscopy (NIRS) [26], blood-oxygen-level-dependent (BOLD) magnetic resonance imaging (MRI), [27] and positron emission tomography (PET) [28]. However, NIRS has relatively poor spatial resolution, and BOLD MRI cannot distinguish the change in sO_2 from that in blood flow. PET needs radioactive isotopes and suffers from poor spatial resolution. OR-PAM, on the other hand, is sensitive to both oxy-hemoglobin (HbO_2) and deoxy-hemoglobin (HbR), and can achieve high resolution, high sensitivity, label-free sO_2 imaging. In this work, we have applied our functional OR-PAM to study the morphological and hemodynamic changes in the brain and skin vessels in response to SNP in vivo. Our results have shown SNP induced a decrease in BP, vasodilation in both brain and skin, as well as two types of sO_2 responses.

2 | MATERIALS AND METHODS

The functional OR-PAM used in this work is shown in Figure 1. The 532 nm light was generated by an Nd: YAG fiber laser (VPFL-G-20, V-Gen, Newport), and the 590 nm

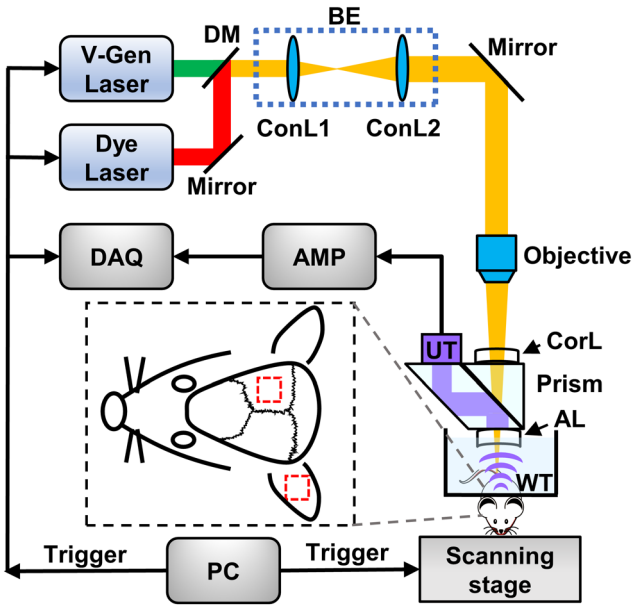

FIGURE 1 Schematic of functional OR-PAM. The inset shows the region of interest on the brain and ear. AL, acoustic lens; AMP, amplifier; BE, beam expander; ConL, convex lens; CorL, correction lens; DM, dichroic mirror; OR-PAM, optical-resolution photoacoustic microscopy; UT, ultrasound transducer; WT, water tank

light was from a dye laser pumped by a 532 nm laser (IS8II-E, EdgeWave, Würselen, Germany). The two laser beams were combined by a dichroic mirror and focused onto the target surface by an objective with an NA of 0.1. A right-angled prism and a rhomboid prism sandwiching a thin layer of silicone oil were assembled for acoustic-optical confocal alignment. An acoustic lens was attached at the bottom of the rhomboid prism for focused acoustic collection. The acoustic lens was submerged in water for acoustic coupling. Aberrations caused by the prisms were compensated with a correction lens attached at the top of the right-angled prism. A water tank was used for ultrasound coupling with deionized water. A thin layer of ultrasound gel was applied between the water tank membrane and the sample surface. 2-D raster scanning was implemented with motorized stages (PLS-85, Physik Instrument, Karlsruhe, Germany). The laser pulse repetition rate was 1 kHz, and the PA signal was recorded with an ultrasonic transducer (central frequency: 30 MHz; one-way −6 dB bandwidth: 45 MHz; V213, Olympus) and sampled by a DAQ card (ATS9350, Alarzar Tech, Canada) with a sampling rate of 250 MHz. The lateral resolution of the OR-PAM system is 3 μm and the axial resolution is 25 μm. Here, we used a shift and sum method for estimating the axial resolution [29].

An SNP solution (Somerset Pharma, New Jersey) was diluted in saline (concentration: 250 μg mL^{-1}). The

solution was prepared immediately before use and kept in a dark environment at 4°C to prevent deterioration [30]. A dose of 75 μg SNP solution was administered through the tail vein. The injection lasts ~15 seconds to avoid acute hypotension-induced heart failure.

In vivo experiments were performed on Swiss Webster mice (male; 8–9 weeks old; ~30 grams in weight). The protocol was approved by the Institutional Animal Care and Use Committee of Duke University. The mouse ear was imaged for studying the skin vessel response. The cortex was imaged to study the brain vessel response. Before the imaging, the mouse was anesthetized with 1.5% isoflurane. A femoral arterial cannulation surgery was performed to monitor systemic BP. The electrocardiogram and BP were continuously recorded with LabChart (ADInstruments Inc., Colorado Springs, CO). The mouse was then transferred to an imaging plate in a prone position, with its head fixed on a tooth bar. A heating pad was placed underneath to maintain the body temperature at 36.5°C, with a real-time temperature probe inserted in the mouse rectum. An incision was made on the scalp to expose the cortical vessels. The skull was intact. In total, 13 mice were imaged: seven mice for brain imaging and six mice for ear imaging. Eleven out of the 13 mice were analyzed for the vessel diameter change, and all the 13 mice were used for the sO_2 change analysis. The remaining two mice of the brain imaging were not included in the vessel diameter analysis due to severe motion artifacts. Motion correction algorithms can be potentially used to improve the image quality [31].

To shorten the scanning time, we used a step size of 5 μm in the fast scanning direction, and 10 μm in the slow scanning direction, which were sufficient to resolve the microvessels in the mouse brain and ear. A 3×3 mm^2 region of interest (ROI) was chosen for both brain and ear imaging, as shown in Figure 1. Each image took 3 minutes. Before SNP injection, control images were acquired as baseline. Hemodynamic responses were repeatedly imaged for 30 minutes after SNP injection. To analyze the vessel diameter, we processed the PA images by using a lab-developed vessel-segmentation algorithm, in which the shortest distance from the vessel centerline to the edge was calculated as the radius. To analyze the sO_2, we calculated the relative concentrations of HbO_2 from the two PA images acquired at 532 nm and 590 nm, using the linear unmixing method reported in the literature [32].

3 | RESULTS

First, we show, that Sodium Nitroprusside (SNP), as expected, caused a substantial decrease in systemic BP through nitric oxide mediated vascular smooth muscle relaxation, leading to systemic vasodilation. Our continuous physiological monitoring shows SNP induced sharp systemic BP decrease of 53% within the first ~1.5 minutes after injection, followed by a recovering time until ~6 minutes. The heart rate initially increased by 7%, returned to the baseline at 3 minutes, and then remained slightly elevated during the experiment. As SNP imposes direct BP suppression through smooth muscle relaxation, the systemic blood flow rate was reduced, leading to an instant compensatory heart rate increase to boost whole body circulation [33–35]. After the SNP-induced effects within the first 1.5 minutes, BP began to recover and the heart rate also started returning to the baseline. Ten out of the 13 mice were used for the BP and heart rate analysis. The remaining three mice were excluded due to recording issues of the physiological monitoring system, as shown in Figure 2.

The OR-PAM images show drastic changes in vessel sizes of the brain and skin vasculature, in response to the SNP induced vasodilation. Figure 3A,B are representative maximum amplitude projection (MAP) images of brain and ear vasculature, respectively. Figure 3C,E are close-up images of the yellow dashed boxes in (A) and (B), respectively, at 0, 3 and 15 minutes after SNP injection. The corresponding segmented images are shown in Figure 3C, with the vessel profiles along the yellow dashed line shown in Figure 3D. Clear vasodilation was observed following SNP injection. For example, the vessel size in Figure 3D increased from 40 μm at the baseline to 50 μm at 3 minutes, and remained at 50 μm at 15 minutes. In the mouse ear (Figure 3E), the arterial vasodilation was more prominent than the venous

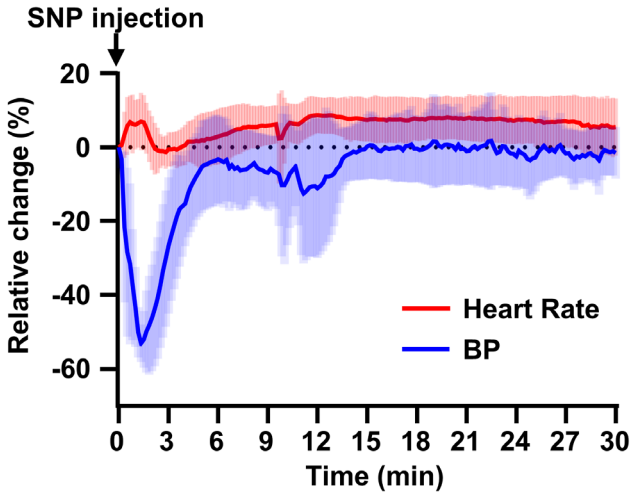

FIGURE 2 Relative change in systemic blood pressure and heart rate induced by SNP (N = 10). Error bars, SD. SNP, sodium nitroprusside

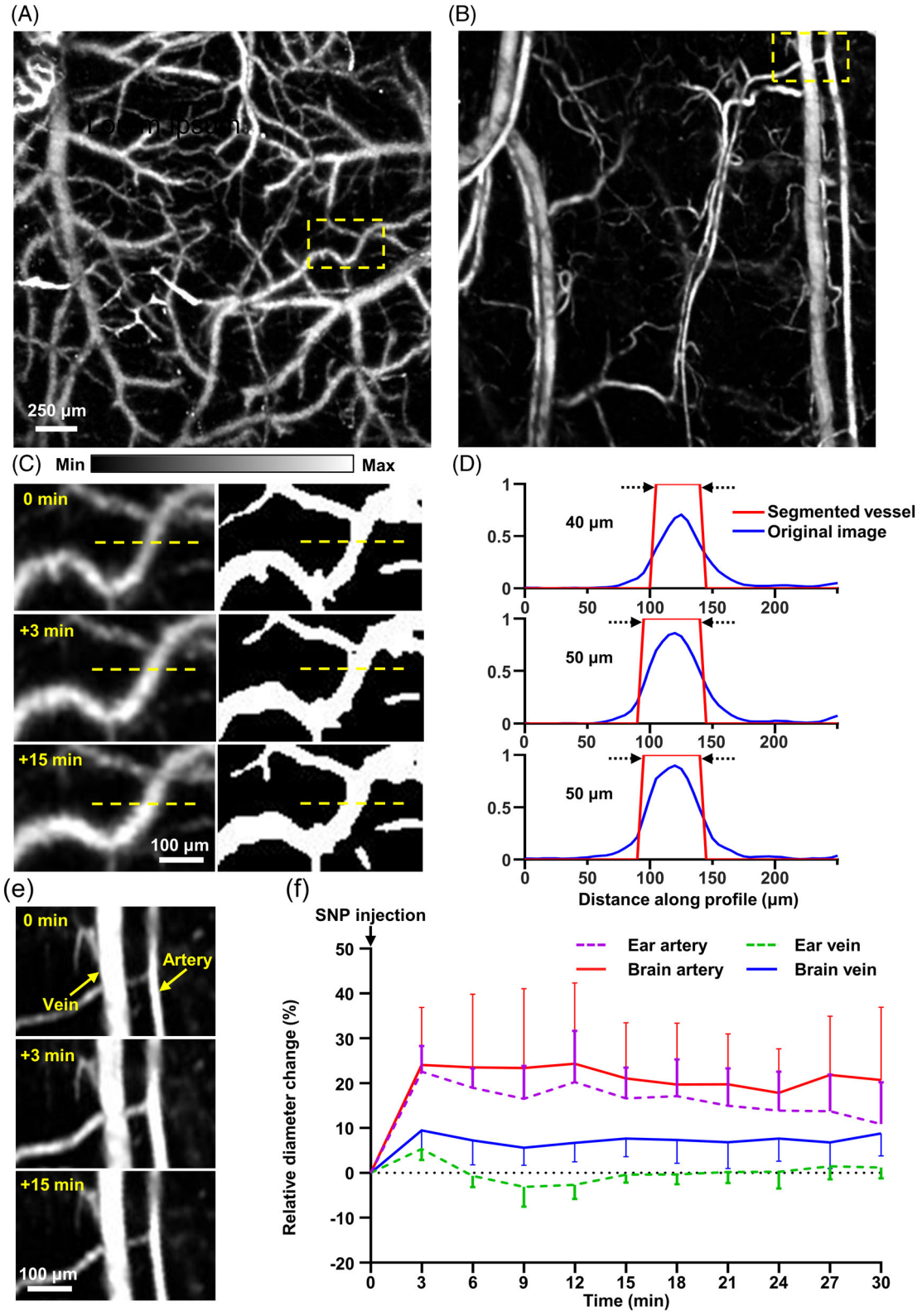

FIGURE 3 SNP induced vasodilation in mouse brain and ear. A, PAM image of cortical vasculature. B, PAM image of ear vasculature. C, Close-up images and segmented vessels of yellow-dashed box in (A) at 0, 3, and 15 minutes after SNP injection. D, Signal profiles of blood vessels and the segmented vessel diameters along the yellow-dashed line in (C) (~40 μm at baseline, ~50 μm at +3 minutes and ~50 μm at +15 minutes). E, Close-up images of the yellow-dashed box in (B) at 0, 3 and 15 minutes after SNP injection. F, Relative diameter changes in the brain (N = 5) and ear (N = 6). Error bars, SD. PAM, photoacoustic microscopy; SNP, sodium nitroprusside

vasodilation, as smooth muscles are mainly distributed around arteries. In total, 11 mice were studied for analyzing the change in vessel size: Five mice for the brain study and six mice for the ear study. Six-eight arteries and four-eight veins per mouse were analyzed. The vessels were randomly selected for quantitative diameter

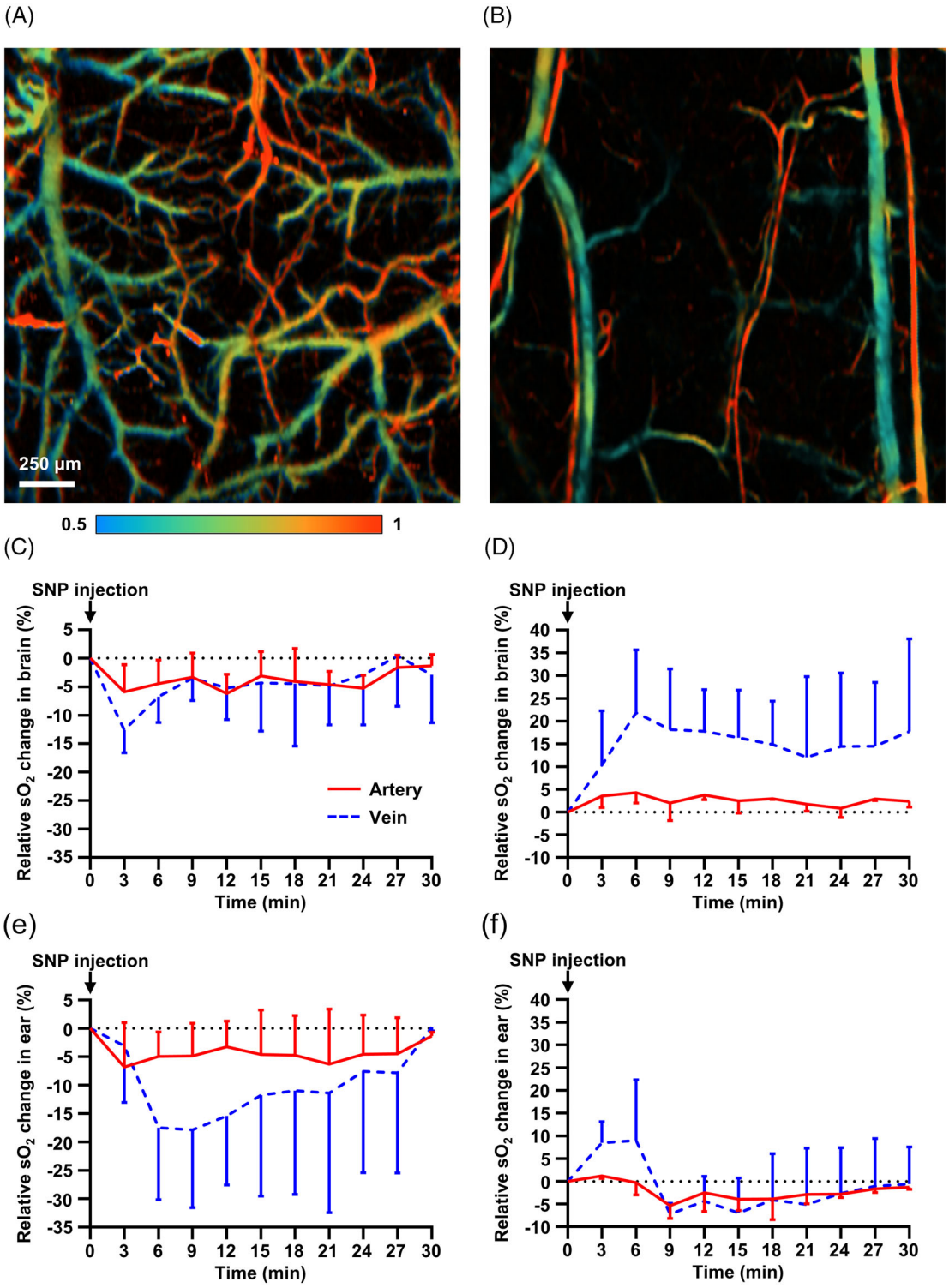

FIGURE 4 Cortical and ear sO_2 response to SNP. A, sO_2 map of brain cortical vasculature. B, sO_2 map of ear vasculature. C, Relative sO_2 decrease in brain (N = 5). D, Relative sO_2 increase in brain (N = 2). E, Relative sO_2 decrease in ear (N = 3). F, Relative sO_2 increase in ear (N = 3). Error bars, SD

analysis. In each mouse, the relative diameter change was quantified and averaged among all the selected vessels. Relative diameter changes across different mice were also averaged, as shown in Figure 3F. The results show that SNP induced an arterial vasodilation of ~24% and ~23% in the brain and ear, respectively. Three minutes after the injection, the arteries started returning to the baseline in both brain and ear. The ear arteries had faster recovery than the brain arteries. The brain and ear veins had an initial vasodilation of 9% and 5%, respectively, followed by recovery between 3 and 9 minutes, at which point the size of ear veins fell below the baseline. Unlike the full recovery in BP by ~6 minutes and in heart rate by ~3 minutes, as shown in Figure 2, the diameters of brain arteries, brain veins, and ear arteries did not fully recover during the observation time. Large fluctuations in vessel sizes of different mice were observed throughout the entire process, mostly due to the different physiological responsiveness among mice. In summary, using OR-PAM, we made several observations on the vessel size following SNP administration: (a) There was clear arterial and venous vasodilation both in the brain and skin; (b) Arterial vasodilation was stronger than venous vasodilation; (c) The skin vasodilation had a faster recovery than the brain; and (d) Compared to the physiological changes shown in Figure 2, the vasodilation lasted longer.

Brain and ear sO_2 maps were also analyzed, as shown in the representative images in Figure 4A,B. We analyzed sO_2 changes in all the 13 mice: seven mice for the brain study and six mice for the ear study. Of note, 4 to 6 arteries and 4 to 6 veins per mouse were randomly selected for quantitative analysis. In each mouse, the relative sO_2 changes in the selected vessels were quantified and averaged. Relative sO_2 changes in all mice were then averaged. Figure 4C,D show the decrease and increase in relative cerebral sO_2 change within 30 minutes of SNP administration, respectively. The majority, five out of seven mice experienced a decrease in cerebral sO_2 (Figure 4C). The sO_2 in arteries and veins decreased by 6% and 13% respectively, at 3 minutes after injection, followed by a quick recovery until 9 minutes. From 9 minutes to 30 minutes, the sO_2 levels of both arteries and veins slowly recovered to the baseline levels. The other two mice showed an increased cerebral sO_2 in response to the SNP injection (Figure 4D). The arterial and venous sO_2 peaked at 6 minutes after injection, with an increase of 4% and 22%, respectively. From 6 minutes to 30 minutes, the sO_2 in veins had a steady recovery until 21 minutes, and a slight elevation for the rest of the time period, while the sO_2 in arteries experienced a moderate recovery to the baseline levels throughout the time period. In the ear imaging, three mice showed decreased sO_2 and the other three mice showed increased changes. Figure 4E depicts the decreased sO_2 change in ear arteries and veins. After SNP administration, the sO_2 in arteries and veins immediately decreased by 7% and 18%, respectively, followed by a gradual recovery. Notably, arterial sO_2 reached the maximum decrease at 3 minutes, while the venous sO_2 reached the minimum at 9 minutes, with a clear delay between the two. As shown in Figure 4F, the arterial and venous sO_2 in the ears of 3 other mice increased by 1% and 9% respectively, followed by a drop below the baseline at 9 minutes. The sO_2 in both arteries and veins then gradually recovered to the baseline level until the end of the 30 minutes time period. Again, a clear delay existed between the venous sO_2 maximum at 6 minutes and the arterial sO_2 maximum at 3 minutes. Compared with the results in the brain, the venous sO_2 response clearly lagged the arterial response in the ear. Again, we observed strong inter-animal differences in physiological responsiveness.

We further examined the correlations among BP, vessel size, and sO_2 responses, as shown in Figure 5. Here, we analyzed only the arterial sO_2 changes. Venous sO_2 changes were excluded from the analysis due to the varied response delay. Following SNP administration, a drastic decrease in BP happened at ~1.5 minutes and a slight decrease happened at ~12 minutes. The changes in vessel size and arterial sO_2 had the same trend as BP in the first 15 minutes after SNP injection. The maximum change in vessel size and arterial sO_2 both happened at 3 minutes. Another mild change in vessel size and arterial sO_2 occurred at 12 minutes. These hemodynamic changes correlated well with the changes in BP. Since the

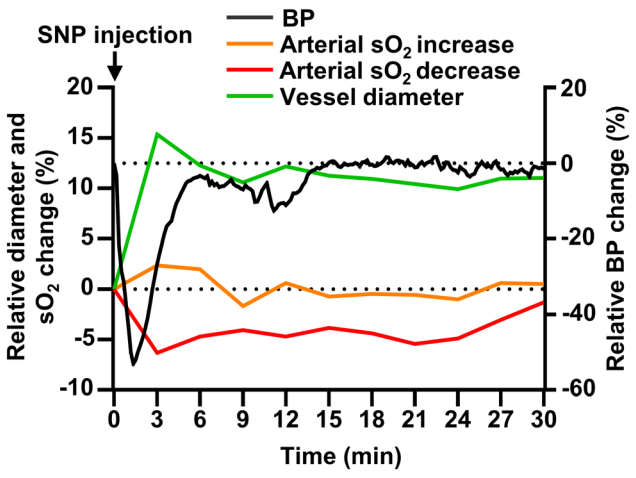

FIGURE 5 Comparison of blood pressure, vessel size and arterial sO_2 change

OR-PAM took one image every 3 minutes, the observed maximum changes had a limited temporal resolution. Overall, we observed that the OR-PAM detected changes in vessel size and arterial sO_2, which closely followed the changes in BP.

4 | DISCUSSION AND CONCLUSION

In this work, we have demonstrated the use of a functional OR-PAM system to study hemodynamic responses to SNP administration in mice in vivo. SNP directly reduced the systemic BP and dilated both arteries and veins in central (brain) and peripheral (ear) vasculature. Decrease and increase in sO_2 were both observed in brain and ear vasculature in response to SNP, and the changes in brain veins closely followed that of the arteries. Changes in vessel size and arterial sO_2 correlated well with changes in BP.

In this study, we observed that SNP induced an acute decrease in the systemic BP, as shown in Figure 2 [33–37]. As reported in previous studies [33, 38, 39], cerebral tissue oxygen (PtO_2) decreased in response to SNP administration, which was attributed to increased arteriovenous shunting and hypotension-induced inadequate capillary perfusion, resulting in relative tissue hypoxia [33, 39]. It was further hypothesized that increased intrapulmonary shunts could contribute to this observation [33, 40]. Previous studies however did not have the ability to assess vessel-by-vessel sO_2 as reported in our study using PAM, and thus could not distinguish sO_2 levels in veins and arteries. If arteriovenous shunting and inadequate capillary perfusion would cause the drop in sO_2 as reported here, we should have observed a higher sO_2 in veins. However, we observed first a decrease in sO_2 in arteries after SNP followed by an even steeper decrease in the associated veins, strongly indicating primarily a decreased oxygen delivery but unchanged oxygen extraction from arteries.

The above dynamics are mirrored in our observation in most animals (five out of seven): SNP first causes a decrease in arterial sO_2 due to pulmonary shunting, as well as a much larger decrease in venous sO_2 due to oxygen extraction. Our data therefore support the hypothesis in earlier studies that SNP increases the intrapulmonary shunting [33, 40]. Since this is a highly variable parameter that depends on the animal size and age, quality of ventilation, as well as the presence of atelectasis, it could explain the inter-animal variability reported in our study. The sO_2 responses in the ear showed similar dynamics, yet the much lower density of capillaries as well as oxygen consumption of the ear cartilage may explain the time delay between arteries and veins, which was different from the "no delay" observation in the brain.

In our opinion, most of our experiments in the brain (five out of seven) also represented the majority of cases observed in clinics, which is further supported by previous studies using intra-parenchymal tissue oxygen sensors. Increased sO_2 after SNP administration on the other hand was previously reported with NIRS monitoring [41–44]. It was believed that both the vasodilation-induced change in arterial to venous blood volume ratio and the actual oxygen balance contributed to the increased NIRS measurements [43].

In our study, we observed intravascular sO_2 increase in two out of seven animals in the brain and ear. Although SNP is an established drug to lower systemic BP, its influence on cerebral blood flow (and for the matter organ perfusion in general) is still unclear. Decreased or increased CBF has both been observed after SNP application [37, 45]. A recent report in healthy subjects even reported an increase blood flow in the middle cerebral artery (MCA) after SNP induced hypotension [45]. If MCA flow in the animals had increased, it could explain the increase in oxygen delivery and explain our observations of increased sO_2. Nevertheless, it still remains an observation in the minority of cases and the actual mechanism of sO_2 increase following SNP administration needs to be investigated in further studies.

We have also demonstrated the potential advantages of OR-PAM. NIRS is a commonly used cerebral oxygenation monitoring technology in preclinical and clinical studies [41, 43, 46, 47]. However, lacking of spatial resolution, NIRS only provides the averaged sO_2 of the mixed volume of arterial and venous blood, rather than sO_2 of individual blood vessels. Increase in arterial to venous blood volume ratio, instead of actual oxygenation change, may also lead to a change in NIRS signals. In contrast, the functional OR-PAM measures sO_2 at single-vessel scale, and can investigate the true oxygenation change in both central and peripheral vasculatures.

However, the current OR-PAM system takes a single image every 3 minutes. We were not able to resolve vasodilation and arterial sO_2 changes between 1.5 and 3 minutes after SNP injection, although the lowest BP happened at ~1.5 minutes. Future work aims to improve functional PA imaging speed that would enable studying the dynamic changes over time [15]. Several fast-scanning mechanisms including the voice-coil stage, MEMS mirror, polygon-mirror scanner, and galvanometer scanner can substantially accelerate the imaging speed. Coupled with the high-speed wavelength tuning [15, 48–53], we expect that OR-PAM can be a valuable

tool to study functional hemodynamics in SNP related research.

ACKNOWLEDGMENTS

This work was partially supported by American Heart Association Collaborative Sciences Award (18CSA34080277). We thank Dr. Caroline Conner for editing the manuscript.

CONFLICTS OF INTEREST

The authors declare no financial or commercial conflict of interest.

DATA AVAILABILITY STATEMENT

The data that support the findings of this study are available from the corresponding author upon reasonable request.

ORCID

Dong Zhang https://orcid.org/0000-0003-2566-7533

REFERENCES

[1] J. Yao, L. Wang, J.-M. Yang, K. I. Maslov, T. T. W. Wong, L. Li, C.-H. Huang, J. Zou, L. V. Wang, *Nat. Methods* **2015**, *12*, 407.
[2] L. Lin, P. Hu, J. Shi, C. M. Appleton, K. Maslov, L. Li, R. Zhang, L. V. Wang, *Nat. Commun.* **2018**, *9*, 2352.
[3] M. Li, B. Lan, W. Liu, J. Xia, J. Yao, *J. Biomed. Opt.* **2018**, *23*, 30506.
[4] M. Chen, H. J. Knox, Y. Tang, W. Liu, L. Nie, J. Chan, J. Yao, *Opt. Lett.* **2019**, *44*, 3773.
[5] T. T. W. Wong, R. Zhang, P. Hai, C. Zhang, M. A. Pleitez, R. L. Aft, D. V. Novack, L. V. Wang, *Sci. Adv.* **2017**, *3*, e1602168.
[6] J.-M. Yang, C. Li, R. Chen, Q. Zhou, K. K. Shung, L. Wang, *J. Biomed. Opt.* **2014**, *19*, 66001.
[7] S. Jeon, J. Kim, D. Lee, J. W. Baik, C. Kim, *Photoacoustics* **2019**, *15*, 100141.
[8] C. Zhang, K. Maslov, L. V. Wang, *Opt. Lett.* **2010**, *35*, 3195.
[9] R. Lin, J. Chen, H. Wang, M. Yan, W. Zheng, L. Song, *Quant. Imaging Med. Surg.* **2015**, *5*, 23.
[10] X. Wang, X. Xie, G. Ku, L. Wang, G. Stoica, *J. Biomed. Opt.* **2006**, *11*, 24015.
[11] J. Yao, K. I. Maslov, Y. Shi, L. A. Taber, L. V. Wang, *Opt. Lett.* **2010**, *35*, 1419.
[12] E. M. Strohm, E. S. L. Berndl, M. C. Kolios, *Photoacoustics* **2013**, *1*, 49.
[13] L. Lin, J. Yao, R. Zhang, C.-C. Chen, C.-H. Huang, Y. Li, L. Wang, W. Chapman, J. Zou, L. V. Wang, *J. Biophotonics* **2017**, *10*, 792.
[14] J. Yao, K. Maslov, Y. Zhang, Y. Xia, L. Wang, *J. Biomed. Opt.* **2011**, *16*, 76003.
[15] B. Lan, W. Liu, Y.-c. Wang, J. Shi, Y. Li, S. Xu, H. Sheng, Q. Zhou, J. Zou, U. Hoffmann, *Biomed. Opt. Express* **2018**, *9*, 4689.
[16] D. G. Hottinger, D. S. Beebe, T. Kozhimannil, R. C. Prielipp, K. G. Belani, *J. Anaesthesiol. Clin. Pharmacol.* **2014**, *30*, 462.
[17] J. A. Friederich, J. F. Butterworth, *Anesth. Analg.* **1995**, *81*, 152.
[18] F. Murad, *J. Clin. Invest.* **1986**, *78*, 1.
[19] H. Ikram, C. J. Low, I. G. Crozier, T. Shirlaw, *Am. J. Cardiol.* **1992**, *69*, 361.
[20] S. Yusuf, S. Macmahon, R. Collins, R. Peto, *Lancet* **1988**, *331*, 1088.
[21] A. Costard-Jäckle, M. B. Fowler, *J. Am. Coll. Cardiol.* **1992**, *19*, 48.
[22] A. K. Vazeery, O. Lunde, *Acta Orthop. Scand.* **1979**, *50*, 433.
[23] I. Vanzetta, A. Grinvald, *Science* **1999**, *286*, 1555.
[24] A. A. Tandara, T. A. Mustoe World, *J. Surg.* **2004**, *28*, 294.
[25] S. S. Foo, D. F. Abbott, N. Lawrentschuk, A. M. Scott, *Mol. Imaging Biol.* **2004**, *6*, 291.
[26] N. N. Tran, M. Tran, E. Elgabalawy, J. Lopez, L. Kysh, *J. Pediatr. Nurs.* **2020**, *55*, 155.
[27] M. Ries, F. Basseau, B. Tyndal, R. Jones, C. Deminière, B. Catargi, C. Combe, C. W. T. Moonen, N. Grenier, *J. Magn. Reson. Imaging* **2003**, *17*, 104.
[28] H. A. Polinder-Bos, J. W. J. Elting, M. J. Aries, D. V. García, A. T. Willemsen, P. J. van Laar, J. Kuipers, W. P. Krijnen, R. H. Slart, G. Luurtsema, *J. Cereb. Blood Flow Metab.* **2020**, *40*, 328.
[29] G. Ku, K. I. Maslov, L. Li, L. V. Wang, *J. Biomed. Opt.* **2010**, *15*, 21302.
[30] I. R. Verner, *Postgrad. Med. J.* **1974**, *50*, 576.
[31] H. Zhao, N. Chen, T. Li, J. Zhang, R. Lin, X. Gong, L. Song, Z. Liu, C. Liu, *IEEE Trans. Med. Imaging* **2019**, *38*, 2139.
[32] H. F. Zhang, K. Maslov, M. Sivaramakrishnan, G. Stoica, L. V. Wang, *Appl. Phys. Lett.* **2007**, *90*, 53901.
[33] W. E. Hoffman, G. Edelman, R. Ripper, H. M. Koenig, *Anesth. Analg.* **2001**, *93*, 166.
[34] M. Lagerkranser, E. Gordon, A. Rudehill, *Acta Anaesthesiol. Scand.* **1980**, *24*, 426.
[35] M. Hamaguchi, T. Ishibashi, N. Katsumata, A. Mitomi, S. Imai, *Cardiovasc. Drugs Ther.* **1992**, *6*, 611.
[36] S. Strandgaard, O. Paulson, *Stroke* **1984**, *15*, 413.
[37] K. Stånge, M. Lagerkranser, A. Sollevi, *Anesth. Analg.* **1991**, *73*, 745.
[38] W. C. Seyde, D. E. Longnecker, *Anesthesiology* **1986**, *64*, 480.
[39] S. K. Ringer, N. G. Clausen, N. Spielmann, S. Ohlerth, A. Schwarz, M. Weiss, *Br. J. Anaesth.* **2018**, *121*, 1308.
[40] P. A. Casthely, S. Lear, J. E. Cottrell, E. Lear, *Anesth. Analg.* **1982**, *61*, 231.
[41] A. T. Moerman, V. M. Vanbiervliet, A. Van Wesemael, S. M. Bouchez, P. F. Wouters, S. G. De Hert, *Anesthesiology* **2015**, *123*, 327.
[42] S. J. E. Lucas, Y. C. Tzeng, S. D. Galvin, K. N. Thomas, S. Ogoh, P. N. Ainslie, *Hypertension* **2010**, *55*, 698.
[43] A. Moerman, W. Denys, F. De Somer, P. F. Wouters, S. G. De Hert, *Br. J. Anaesth.* **2013**, *111*, 619.
[44] T. Kurita, S. Kawashima, K. Morita, Y. Nakajima, *Eur. J. Anaesthesiol. EJA* **2019**, *36*, 531.
[45] N. D. Olesen, M. Fischer, N. H. Secher, *J. Physiol.* **2018**, *596*, 3967.
[46] J. M. Stewart, M. S. Medow, A. DelPozzi, Z. R. Messer, C. Terilli, C. E. Schwartz, *Am. J. Physiol. Heart Circ. Physiol.* **2013**, *304*, H1576.

[47] H. M. Watzman, C. D. Kurth, L. M. Montenegro, J. Rome, J. M. Steven, S. C. Nicolson, *Anesthesiology* **2000**, *93*, 947.
[48] J. Lee, S. Han, D. Seong, J. Lee, S. Park, R. E. Wijesinghe, M. Jeon, J. Kim, *Opt. Lett.* **2020**, *45*, 865.
[49] L. Wang, K. Maslov, J. Yao, B. Rao, L. V. Wang, *Opt. Lett.* **2011**, *36*, 139.
[50] J. Yao, L. Wang, J.-M. Yang, L. S. Gao, K. I. Maslov, L. V. Wang, C.-H. Huang, J. Zou, *J. Biomed. Opt.* **2012**, *17*, 80505.
[51] J. Chen, Y. Zhang, L. He, Y. Liang, L. Wang, *Photoacoustics* **2020**, *20*, 100195.
[52] J. Y. Kim, C. Lee, K. Park, G. Lim, C. Kim, *Sci. Rep.* **2015**, *5*, 1.
[53] C. Zhang, H. Zhao, S. Xu, N. Chen, K. Li, X. Jiang, L. Liu, Z. Liu, L. Wang, K. K. Y. Wong, J. Zou, C. Liu, L. Song, *Opt. Lett.* **2020**, *45*, 4312.

How to cite this article: Zhang D, Li R, Chen M, et al. Photoacoustic imaging of in vivo hemodynamic responses to sodium nitroprusside. *J. Biophotonics*. 2021;e202000478. https://doi.org/10.1002/jbio.202000478